Rapid endogenic rock recycling in magmatic arcs

Junyong Li
Nanjing University
Ming Tang
Peking University/Rice University
Cin-Ty Lee
Rice University
Xiaolei Wang (wxl@nju.edu.cn)
Nanjing University https://orcid.org/0000-0002-5115-7804
Zhi-Dong Gu
Research Institute of Petroleum Exploration and Development
Xiao-Ping Xia
State Key Laboratory of Isotope Geochemistry, Guangzhou Institute of Geochemistry, Chinese Academy of Sciences, Guangzhou 510640, China https://orcid.org/0000-0002-3203-039X
Di Wang
Nanjing Univeristy
De-Hong Du
Nanjing Univeristy
Lin-Sen Li
Nanjing Univeristy

Article

Keywords: thrust faults, endogenic recycling, phase equilibria modelling, magmatic arcs

DOI: https://doi.org/10.21203/rs.3.rs-50308/v1

Abstract

In subduction zones, materials on Earth's surface can be transported to the deep crust or mantle, but the exact mechanisms and the nature of the recycled materials are not fully understood. Here, we report a set of migmatites from western Yangtze Block, China. These migmatites have similar bulk compositions as forearc sediments. Zircon age distribution and Hf–O isotopes indicate that the precursors of the sediments were predominantly derived from juvenile arc crust itself. Using phase equilibria modelling, we show that the sediments experienced high temperature-to-pressure ratio metamorphism and were most likely transported to deep arc crust by intracrustal thrust faults. By dating the magmatic zircon cores and overgrowth rims, we find that the entire rock cycle, from arc magmatism, to weathering at the surface, then to burial and remelting in the deep crust, took place within ~ 10 Ma. Our findings highlight thrust faults as an efficient recycling channel in compressional arcs and endogenic recycling as an important mechanism driving internal redistribution and differentiation of arc crust.

Introduction

Magmatic arcs witness the interplay between endogenous and exogenous processes, including magmatism, crustal thickening, uplift, erosion, sedimentation and burial of detritus[1–4]. Magmatism produces new crust, which later interacts with the hydrosphere and atmosphere through erosion and weathering. On the other hand, crustal materials from the surface are recycled to Earth's interior. This chain of processes in magmatic arcs play important roles in driving much of the mass exchange between Earth's interior and surface. The inward transport of surface materials, including volatiles, has profound influence on the cycling of carbon, oxygen, sulfur, etc. on Earth's surface and may alter the chemical and physical properties of the deep crust and even mantle.

Nearly every Phanerozoic arc in the world exhibit crustal signatures in geochemistry, suggesting pervasive crustal recycling in the formation of arc crust. Conventional views link crustal recycling processes to slab subduction, including sediment subduction and subduction erosion (± relamination) have been widely invoked to explain the crustal signatures seen in most arc magmas[5,6]. Yet the recent work on continental arcs hints at thrust faults as potential recycling channels[7,8 9]. Here, we examined a suite of migmatites from a Neoproterozoic magmatic arc in western China. We used combined petrologic, geochronologic and geochemical studies of these samples to understand the nature of the recycled materials and evaluate how thrust faults may contribute to rock recycling in compressional arc settings.

Geological setting and samples

Western margin of the Yangtze Block became tectonically active since the early Neoproterozoic. Intra-oceanic arc magmatism started before 971±16 Ma[10] and then transitioned to Andean-type magmatism at ca. 870 Ma[11]. This prolonged magmatic history gave rise to linearly distributed arc magmatic rocks spanning over 800 km at present coordinate (Fig. S1a). Post-Triassic orogenic process along the Longmenshan Thrust Belt[12] exposed numerous Neoproterozoic plutonic complexes in western Yangtze

Block, of which the largest one is known as the Pengguan Complex, comprising voluminous 860–750 Ma plutonic rocks (Fig. S1b). The Huangshuihe Group in the core region of the Pengguan Complex serves as a huge roof pendant and consists of metamorphic rocks of schist, quartzite and pyroclastic rock. Ductile deformation, faults, mylonite with S-C fabric, and migmatitic lineation are extensive in the sequences (Fig. S2).

Six migmatite and one leucosome samples in the Huangshuihe Group were collected in this study. The migmatites contain compositional layering, local carbonate interlayer and was intruded by mafic dikes (Fig. S2). Patch-shaped neosomes are abundant in the migmatites (Fig. S2) and formed during incipient partial melting. Large leucosomes (around 50 cm width) occur occasionally and are usually fed by a few small leucosome veins.

The main minerals in migmatite are plagioclase, biotite, K-feldspar, quartz and muscovite (Fig. S3). Anatexis of primary mineral assemblage lead to prevalent zircon overgrowth and muscovite-rimmed biotite in the migmatite (Fig. S3&5). Entrainment of peritectic phase, which consists of small spessartine-rich garnet grains, biotite, muscovite, quartz, plagioclase, K-feldspar and Fe-oxides, was found in 16YX-1-1(Fig. S3; Table S4). The reaction of "biotite + MnO, Al_2O_3, SiO_2 (from melt) = garnet + muscovite"[13] may control garnet paragenesis. These observations are indicative of near-solidus partial melting with local melt segregation.

Results

Most zircon grains in the Pengguan migmatites have core-rim structures. The zircon core domains, presumably derived from arc magmatic detritus, show limited variation in their ages, concentrating at ~ 830–870 Ma, with few at ~ 930 Ma (Fig. 1a), and have mantle-like to slightly elevated $\delta^{18}O$ values (5.3 to 7.4‰) (Fig. 1b). Their $\varepsilon_{Hf}(t)$ values vary from − 3 to + 13, with most being positive, indicative of heterogeneous but generally juvenile sources. Zircon overgrowth rims are slightly younger than the maximum depositional age for each sample, with U − Pb dates generally ranging from ~ 815 Ma to ~ 860 Ma (Table S3). The overgrowth rims have significantly higher $\delta^{18}O$ values (9.3 to 13.3‰) compared with those of core domains, despite their similar $\varepsilon_{Hf}(t)$ range (−3 to + 8 except one analysis of − 9) as core domains (Table S2). Zircon from the leucosome sample show homogeneous $\delta^{18}O$ values (11.1 to 13.4‰) with a large range of $\varepsilon_{Hf}(t)$ values (-6.9 to + 8.4) (Table S2). All $\varepsilon_{Hf}(t)$ values were calculated to t = 850 Ma in order to facilitate comparison.

We reconstructed the metamorphic P-T conditions for the Pengguan migmatites using Perple_X 6.9.0 (http://www.perplex.ethz.ch*).* The bulk rock composition of sample 16YX-1-1 was chosen for calculation because this sample clearly documents: 1) mineral-melt interaction; 2) coexistence of minerals (Mn-rich garnet + biotite + muscovite + quartz + plagioclase + K-feldspar + Fe-oxides) and; 3) minor partial melting with no evident melt migration. In the calculated P-T pseudosection, the mineral assemblage of the Pengguan migmatite falls in a narrow domain (domain 1 in Fig. 2a) near the solidus. Using Si pfu in muscovite from 16YX-1-1 (3.08 to 3.14, in moles per formula unit; Table S4), which is sensitive to

pressure in the K-feldspar + phlogopite + quartz system[15], we further constrained the anatexis P–T conditions to ~ 670 °C and 5.9 – 8.1 kbar (Fig. 2). The low anatexis temperature is also consistent with the extremely low Th/U ratios of the zircon overgrowth rims (Fig. 1a). At near-solidus temperatures, Th concentration in the melt is largely buffered by Th-rich accessory minerals (such as monazite and allanite)[16].

Discussion

Forearc magmatic detritus as protolith of migmatite

The Pengguan migmatites are peraluminous with aluminum saturation indices (ASI) of 1.10–1.44 (Table S1). Muscovite and peritectic garnets are observed in all samples, indicating peraluminous composition of the protoliths. These migmatites also show geochemical signatures similar to those arc magmatic rocks and forearc sediments from Peninsular Ranges batholith, but distinct from those of MORB and intraplate volcanics (Fig. 3), suggesting that the protoliths of these migmatites are dominated by arc-related magmatic detritus. This view is also consistent with the observation that the magmatic cores of zircons in the migmatites have very similar age distributions to that of the arc-related magmatic rocks in the study area (Fig. 1a). The consistent and juvenile Hf isotopes of the zircon cores and overgrowth rims lends further support for the arc origin of the migmatite precursor materials. We thus suggest the Pengguan migmatites documented a process that recycled the arc crust itself, and we refer to this process as endogenic recycling to distinguish it from recycling of oceanic sediments or oceanic crust into subduction zones.

We note that the zircon overgrowth rims have systematically higher $\delta^{18}O$ values than the magmatic cores (Fig. 1b) which is indicative of equilibrium with the high-$\delta^{18}O$ anatectic melts during crystallization. High $\delta^{18}O$ is a diagnostic signature of low-temperature water-rock interaction at Earth's surface. Thereby the protoliths of the Pengguan migmatites must have undergone some extent of chemical weathering and O isotope exchange at low temperatures before being buried and remelted.

Intra-arc thrust faults as rapid endogenic recycling channels

An important question pertains to how the magmatic detritus that had been initially deposited at the surface was transported to the hot deep crust. In magmatic arc settings, recycling of surface rocks has generally been associated with slab subduction. Subducting slabs can directly bring trench sediments to the deep crust or even mantle[5,6]. Subduction erosion has also been recognized as an important mechanism for downward transport of shallow crustal materials[5]. Slab tops are cold (dT/dP = 16–64 ºC/kbar) (Fig. 2b; estimated from Penniston-Dorland et al.[20]) and melting of the sediments deposited at the slab surface is generally considered difficult at crustal depths[24]. Phase equilibrium modelling shows that the Pengguan migmatites formed at ~670 ºC and 5.9–8.1 kbar. These P–T conditions translate into a hot geothermal gradient of 83–114 ºC /kbar or 25 to 34 ºC /km, considerably hotter than slab top geothermal gradients but consistent with those seen in arc crust with continuous magmatic inflation[19]

(Fig. 2b). This would imply that the Pengguan forearc detrital sediments, shortly after their deposition, were rapidly transported to the deep crust beneath the active arc volcanic front. We suggest the most likely recycling mechanism is via deep thrust faults in the upper continental plate rather than by slab subduction (Fig. 4). In compressional magmatic arcs, including mature island arcs and continental arcs, fold and thrust belts may extensively develop in the forearc and inboard side of the arc and serve as important crustal recycling channels. Typical examples include the thrust fault systems in Lachlan orogen[25], Japan arc[26] and the Cordilleran continental arc system[7].

The nearly identical age distributions of the zircon cores and overgrowth rims (Fig. 1a) hint at a fast rock cycle, from arc magmatism to water-rock interaction, then to burial and remelting. To estimate the timescale and rate of burial for the Pengguan forearc magmatic detritus, we took the weighted average value of the 50% of youngest U–Pb dates with concordant U–Th–Pb isotopes from zircon core domains as the maximum depositional age, and the weighted average age of zircon rims as the remelting (anatexis) age (Table S2; Fig. 1a). In doing so, we see that the maximum depositional ages are less than 7 to 14 Ma older than the remelting ages for each sample. This means that the magmatic protoliths of the Pengguan forearc sediments were exhumed, deposited in a sedimentary basin, and then buried to the depth of crustal anatexis all within ~ 10 Ma. This implies an efficient burial process with minimum burial rate of 2–3 mm/y.

Implications

Our findings point to endogenic recycling as an important mechanism driving internal redistribution of arc crustal materials, but its role in the formation of arc crust may have been largely overlooked in the past. Radiogenic isotopes are widely employed to constrain crustal recycling processes, but given the short residence time (e.g., 10 Ma), radiogenic isotopes can be completely blind to endogenic recycling. We speculate that extensive endogenic recycling may also generate significant decoupling between radiogenic and stable isotope compositions in recycled materials and their derivative melts.

Rapid endogenic recycling may be facilitated by thrust fault networks. Deep thrust faults may serve as critical transport channels connecting the surface and deep arc crust with ongoing magmatism. Endogenic recycling enhances the overall differentiation of arc crust, and because large-scale thrust faults necessarily form in compressional settings, efficient endogenic recycling may partly explain why thick arc crust formed in compressional settings (e.g., continental arcs) tend to be more differentiated than thin arc crust formed in extensional settings (e.g., immature island arcs) [27].

Methods

In situ Zircon isotopes Zircon grains were separated using conventional density and magnetic techniques, mounted in epoxy resin disk, and polished to section the crystals in about half. In situ U–Th–Pb–Hf–O isotope analyses were carried out guided by cathodoluminescence (CL) images and transmitted and reflected photographs. Each group of U–Th–Pb–Hf–O isotopic analysis was designed to conduct on same or similar domain from one zircon. Zircon oxygen isotopes and U–Pb ages were analyzed using the

Cameca IMS-1280HR second ion mass spectrometry (SIMS) at the Guangzhou Institute of Geochemistry, Chinese Academy of Sciences. The disk surface was vacuum-coated with high-purity gold prior to SIMS analysis. Detailed SIMS analytical procedures resemble those described in Li et al. (2009, 2010, 2017) [28–30]. After U–Pb dating, the sample mount was re-ground for ~5μm to ensure any oxygen implanted in zircon surface from the O_2^- beam used for U–Pb analysis is completely removed before O isotopic analysis. The measured U–Pb–O isotopic data were corrected for instrumental mass fractionation (IMF) using the Penglai zircon standard[29]. Uncertainties of SIMS U–Pb–O results were monitored using zircon Qinghu standard[31]. Our analyzed average $^{238}U/^{206}Pb$ age and $\delta^{18}O$ value of zircon Qinghu standard are 159±2 Ma (n=9; 1σ) and 5.32±0.25‰ (n=32; 2σ) respectively, consistent within errors to reported values of 159±0.2 Ma and 5.3±0.3‰[31]. Oxygen isotope ratios are expressed in the standard $\delta^{18}O$ notation, signifying deviation of the measured $^{18}O/^{16}O$ value from Vienna standard mean ocean water ($^{18}O/^{16}O$= 0.0020052; Baertschi[32]) in parts per thousand. Zircon Lu–Hf isotopic analyses were conducted using a GeoLas 193nm laser-ablation system attached to a Neptune (Plus) MC-ICP-MS at State Key Laboratory for Mineral Deposits Research of Nanjing University (MiDeR-NJU). Detailed analytical procedures for zircon Hf isotopes are similar to those in Griffin et al. (2000, 2006) [33,34]. We use zircon standard Mud Tank ($^{176}Hf/^{177}Hf$ = 0.282507±0.000006 [35]) to evaluate the reliability of the data during the course of experiment. Beam diameter of 44 μm was preferentially adopted to zircon domain with large size, while 32 μm beam diameters was adopted to zircon domain with its size < 44 μm. Each diameter-change operation will be followed by analysis of zircon standard to ensure the stability of the experiment. Ablation pulse rate and energy density are 10 Hz and 10.5 J/cm^2 respectively. The detailed analytical results and their related calculation process are listed in the Supplementary Table S3.

Whole-rock geochemistry Major elements were analysed using a Thermo ARL9900XP X–ray fluorescence spectrometer (XRF) at the MiDeR-NJU. The analytical precision is generally better than 2% for all elements. Whole-rock rare earth and other trace elements were analyzed using an ICP-MS (Finnigan MAT–Element II) instrument at MiDeR-NJU. Each sample was precisely weighted 30 mg and then was put into a 15 ml Savillex digestion vessel. After being dissolved by HNO3 and the injection of 1 ml 500 ng/ml internal standard Rh solutions, the samples are ready for analyzing. Analytical precision for most elements by ICP- MS is better than 5%. Major and trace element composition data of the migmatite and leucosome samples are provided in Supplementary Table S1.

Mineral Composition The mineral major element compositions were determined using a JEOL 53 JXA-8100 electron probe microanalysis (EPMA) at the MiDeR-NJU. The instrument was operated in wavelength-dispersion mode with a beam diameter of 1–2 μm, a 15kV accelerating voltage, and a 20 nA beam current. Element peaks and backgrounds were measured for all elements with counting times of 10 and 5. Natural and synthetic standards were used. Detection limits were better than 0.02 wt % for the oxides of most elements. All EPMA data were automatically reduced using the ZAF correction program. Mineral major content results are provided in Supplementary Table S4.

Data availability

Major and trace element composition data of the migmatite and leucosome samples are provided in Supplementary Table S1. Summary and details of Age-$\delta^{18}O$-$\varepsilon_{Hf}(t)$ results from core and rim zircon of the migmatites are provided in Supplementary Table S2 and S3, respectively. Mineral major content results are provided in Supplementary Table S4.

Declarations

Acknowledgements

This work was financially supported by the State Key R&D Project of the Ministry of Science and Technology of China (2016YFC0600203), the Fundamental Research Funds for the Central Universities (020614380089) and the Dengfeng Project of Nanjing University to XLW, and the scholarship from China Scholarship Council (File No. 201806190157) to JYL.

Author contributions

J.Y.L. initiated the idea, collected samples, conducted whole-rock and mineral analyses and carried out melting modeling. J.Y.L., M.T., C.-T.A.L and X.L.W. wrote the manuscript. X.L.W. designed the project. X.P.X. contributes to SIMS analyses. Z.D.G., D.W., and D.H.D assisted in sample collection. L.S.L. helped in melting modeling. All authors contributed to data interpretation.

References

1. Lackey, J. S., Valley, J. W. & Saleeby, J. B. Supracrustal input to magmas in the deep crust of Sierra Nevada batholith: Evidence from high-$\delta^{18}O$ zircon. *Earth Planet. Sci. Lett.* 235, 315–330 (2005).
2. Ducea, M. N., Saleeby, J. B. & Bergantz, G. The Architecture, Chemistry, and Evolution of Continental Magmatic Arcs. *Annual Rev. Earth Planet. Sci.* 43, 299–331 (2015).
3. Lee, C.-T. A., Thurner, S., Paterson, S. & Cao, W. R. The rise and fall of continental arcs: Interplays between magmatism, uplift, weathering, and climate. *Earth Planet. Sci. Lett.* 425, 105–119 (2015).
4. Jiang, H. H. & Lee, C.-T. A. Coupled magmatism–erosion in continental arcs: Reconstructing the history of the Cretaceous Peninsular Ranges batholith, southern California through detrital hornblende barometry in forearc sediments: *Earth Plane. Sci. Lett.* 472, 69–81 (2017).
5. von Huene, R. & Lallemand, S. Tectonic erosion along the Japan and Peru convergent margins. *Geol. Soc. Am. Bull.* 102, 704–720 (1991).
6. Hacker, B. R., Kelemen, P. B. & Behn, M. D. Differentiation of the continental crust by relamination. *Earth Planet. Sci. Lett.* 307, 501–516 (2011).
7. DeCelles, P. G., Ducea, M. N., Kapp, P. & Zandt, G. Cyclicity in Cordilleran orogenic systems. *Nature Geoscience.* 2, 251–257 (2009).
8. Ducea, M. N. & Chapman, A. D. Sub-magmatic arc underplating by trench and forearc materials in shallow subduction systems: A geologic perspective and implications. *Earth-Sci. Rev.* 185, 763–779

(2018).

9. Pearson, D. M. et al. Sediment underthrusting within a continental magmatic arc: Coast Mountains batholith, British Columbia. *Tectonics* 36, 2022–2043 (2017).
10. Li, J. Y., Wang, X. L. & Gu, Z. D. Early Neoproterozoic arc magmatism of the Tongmuliang Group on the northwestern margin of the Yangtze Block: Implications for Rodinia assembly. *Precamb. Res.* 309, 181–197 (2018).
11. Zhao, J. H., Li, Q.W., Liu, H. & Wang, W. Neoproterozoic magmatism in the western and northern margins of the Yangtze Block (South China) controlled by slab subduction and subduction-transform-edge-propagator. *Earth-Sci. Rev.* 187, 1–18 (2018).
12. Deng, B. et al. Sedimentary record of Late Triassic transpressional tectonics of the Longmenshan thrust belt, SW China. *J. Asian Earth Sci.* 48, 43–55 (2012).
13. Miller, C. F. & Stoddard, E. F. The Role of Manganese in the Paragenesis of Magmatic Garnet: An Example from the Old Woman-Piute Range, California. *J. Geol.* 89, 233–246 (1981).
14. Valley, J. W. et al. 4.4 billion years of crustal maturation: Oxygen isotope ratios of magmatic zircon. *Contrib. Mineral. Petrol.* 150, 561–580 (2005).
15. Massonne, H. J. & Szpurka, Z. Thermodynamic properties of white micas on the basis of high-pressure experiments in the systems K_2O-MgO-Al_2O_3-SiO_2-H_2O and K_2O-FeO-Al_2O_3-SiO_2-H_2O. *Lithos* 41, 229–250 (1997).
16. Yakymchuk, C., Kirkland, C. L. & Clark, C. Th/U ratios in metamorphic zircon. *J. Meta. Geol.* 36, 715–737 (2017).
17. Holland, T. J. B. & Powell, R. An improved and extended internally consistent thermodynamic dataset for phases of petrological interest, involving a new equation of state for solids. *J. Meta. Geol.* 29, 333–383 (2011).
18. Rothstein, D. A. & Manning, C. E. Geothermal gradients in continental magmatic arcs; constraints from the eastern Peninsular Ranges Batholith, Baja California, Mexico. *Geol. Soc. Am. Spec. Paper* 374, 337–354 (2003).
19. Hopkins, M., Harrison, T. M., & Manning, C. E. Low heat flow inferred from > 4 Gyr zircons suggests Hadean plate boundary interactions. *Nature* 456, 493–496 (2008).
20. Penniston-Dorland, S. C., Kohn, M. J. & Manning, C. E. The global range of subduction zone thermal structures from exhumed blueschists and eclogites: rocks are hotter than models. *Earth Planet. Sci. Lett.* 428, 243–254 (2015).
21. Lee, C.-T. A., Morton, D. M., Kistler, R. W. & Baird, A. K. Petrology and tectonics of Phanerozoic continent formation: from island arcs to accretion and continental arc magmatism. 370–387 (2007).
22. Jiang, H. H. & Lee, C.-T. A. On the role of chemical weathering of continental arcs in long-term climate regulation: A case study of the Peninsular Ranges batholith, California (USA). L115733 (2019).
23. Pearce, J. A. Geochemical finger printing of oceanic basalts with applications to ophiolite classification and the search for Archean oceanic crust. 14–48 (2008).

24. Johnson, M.C. & Plank, T. Dehydration and melting experiments constrain the fate of subducted sediments. *Geochem. Geophys. Geosyst.* 1, GC000014 (1999).
25. Foster, D. A., & Gray, D. R. The structure and evolution of the Lachlan Fold Belt (Orogen) of eastern Australia. *Annual Rev. Earth Planet. Sci.* 28, 47–80 (2000).
26. Isozaki, Y. Anatomy and genesis of a subduction-related orogen: a new view of geotectonic subdivision and evolution of the Japanese islands. *Island Arc* 5, 289–320 (1996).
27. Farner, M. J. & Lee, C.-T. A. Effects of crustal thickness on magmatic differentiation in subduction zone volcanism: A global study. E*arth Planet. Sci. Lett.* 470, 96–107 (2017).
28. Li, X. H., Liu, Y., Li, Q. L., Guo, C. H. & Chamberlain, K. R. Precise determination of Phanerozoic zircon Pb/Pb age by multicollector SIMS without external standardization. *Geochem. Geophys. Geosyst.* 10, 573–575 (2009).
29. Li, X. H. et al. Penglai zircon megacrysts: A potential new working reference material for microbeam determination of Hf-O isotopes and U-Pb age. *Geostand. Geoanalyt. Res.* 34, 117–134 (2010).
30. Li, W.J. et al. Paleoproterozoic S-type granites from the Helanshan Complex in Inner Mongolia: Constraints on the provenance and the Paleoproterozoic evolution of the Khondalite Belt, North China Craton. *Precamb. Res.* 299, 195–209 (2017).
31. Li, X. H. et al. Qinghu zircon: A working reference for microbeam analysis of U-Pb age and Hf and O isotopes. *Chin. Sci. Bull.* 58, 4647–4654 (2013).
32. Baertschi, P. Absolute ^{18}O content of standard mean ocean water. *Earth Planet. Sci. Lett.* 31, 341–344 (1976).
33. Griffin, W. L. et al. The Hf isotope composition of cratonic mantle: LA-MC-ICP-MS analysis of zircon megacrysts in kimberlites. *Geochim. Cosmochim. Acta* 64, 133–147 (2000).
34. Griffin, W. L., Belousova, E. A., Walters, S. G. & O'Reilly, S. Y. Archean and Proterozoic crustal evolution in the eastern succession of the Mt Isa district Australia: U–Pb and Hf isotope studies of detrital zircons. *Aust. J. Earth Sci.* 53, 125–149.
35. Woodhead, J. D. & Hergt, J. M. A preliminary appraisal of seven natural zircon reference materials for in situ Hf isotope determination. *Geostand. Geoanal. Res.* 29, 183–195.

Figures

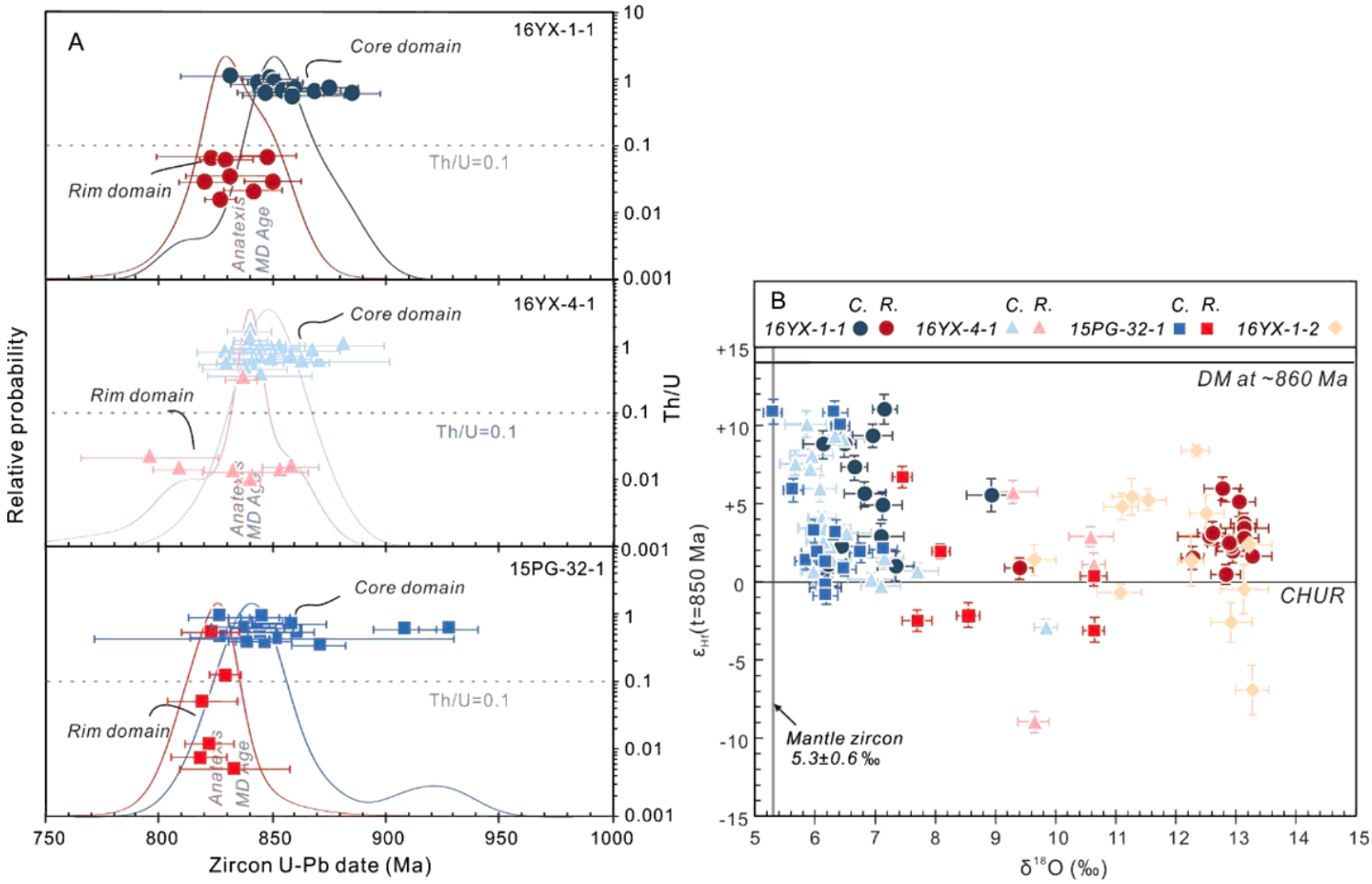

Figure 1

Zircon U–Pb age distributions and zircon δ18O-εHf(t) values of the Pengguan migmatites. a Core and rim age distribution of zircon extracted from Pengguan migmatites. Unimodal core and rim zircon U-Pb dates distribution is shown in the diagram. Anatexis and maximum depositional ages (MD Age, see discussion for the calculation) of each sample are marked with light red and blue, respectively. Zircon U–Pb dates with concordant U–Th–Pb isotopes were used here. Concordant criteria are given in Table S3. b δ18O-εHf(t = 850 Ma) diagram for core and rim domains of three migmatite samples and zircon from leucosome. C. = core domain, R. = rim domain. Mantle zircon δ18O = 5.3±0.6 ‰14.

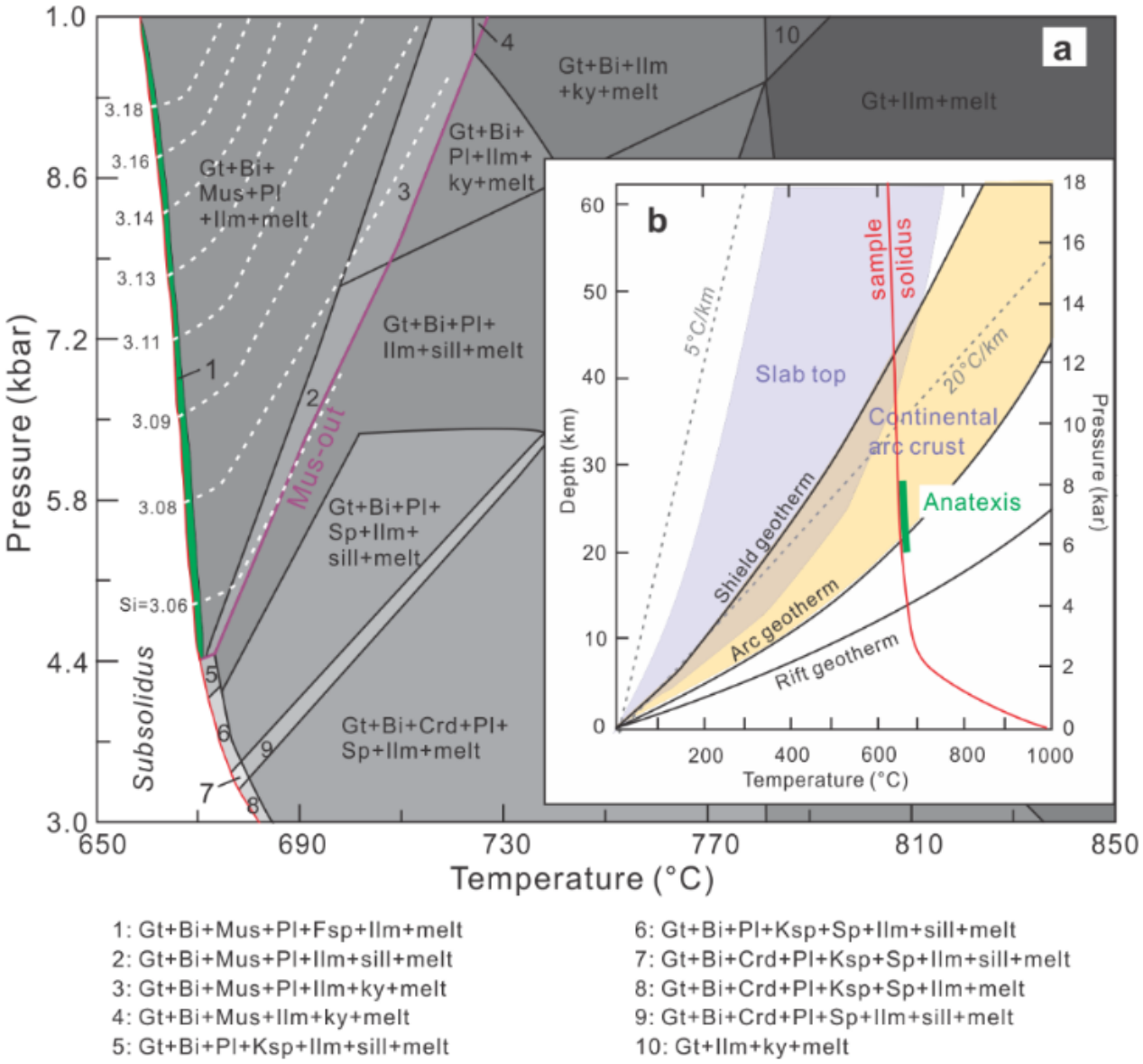

Figure 2

Reconstructed anatexis P-T conditions for the Pengguan migmatites. a P–T pseudosection calculated for the Pengguan migmatite (16YX-1-1) in the MnNKCFMASH system (Quartz and H2O in excess). Internally consistent thermodynamic dataset of Holland and Powell17 was used. Mineral assemblage in the thin green belt along the solidus is consistent with the mineral composition and field observations of sample 16YX-1-1. The predicted Si isopleths content in muscovite (3.06–3.18, in molar per formula unit) are shown by the white dotted lines. Gt–garnet, Bi–biotite, Mus–muscovite, Pl–plagioclase, Fsp–K-feldspar, Ilm–ilmenite, sil–sillimanite, ky–kyanite, Sp–spinel, Crd–cordierite. b P-T conditions of the Pengguan migmatite formation (green line) projected on geothermal gradients in various geologic settings (modified after Rothstein and Manning18, Hopkins et al.19 and Penniston–Dorland et al.20).

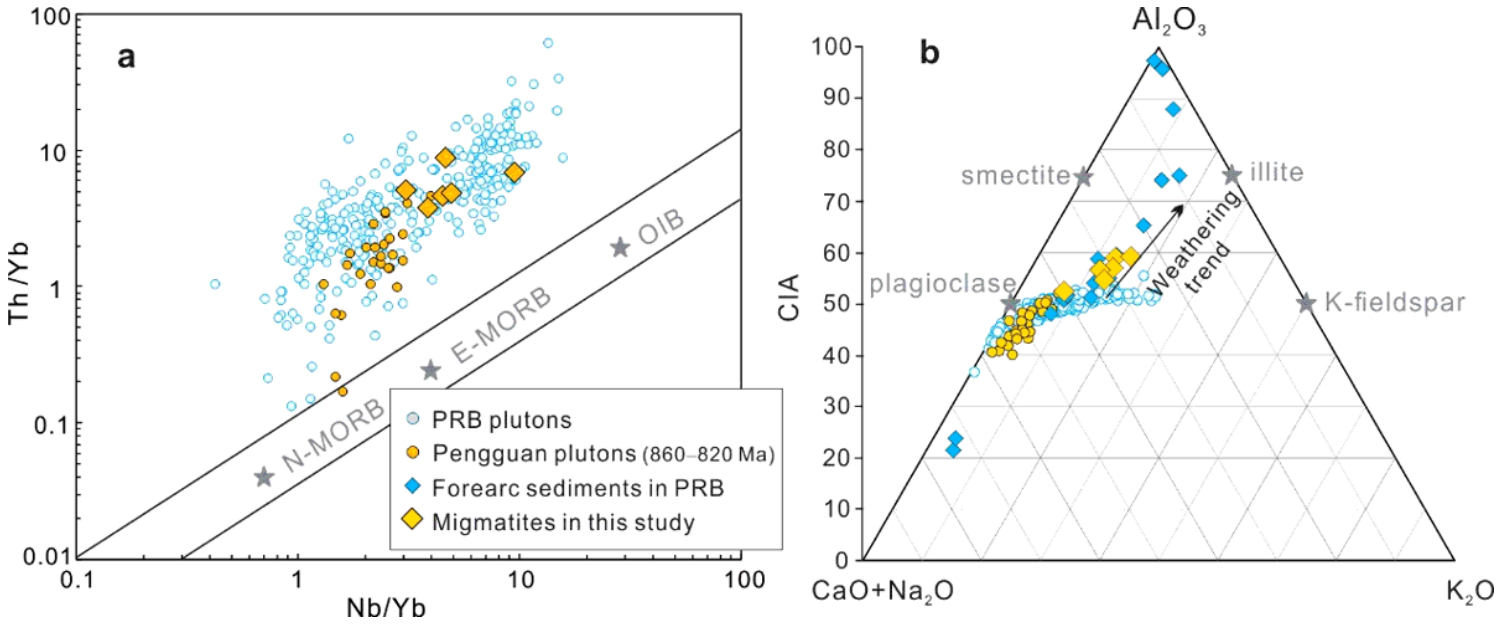

Figure 3

Geochemical affinity of the Pengguan migmatites compared with those of 860–820 Ma plutonic rocks nearby, the plutonic rocks from Peninsular Ranges batholith (PRB)21 and forearc sediments derived from PRB22. The Nb/Yb-Th/Yb discrimination diagram is after Pearce23 and the A–CN–K–CIA (Chemical index of alteration) diagram is after Jiang and Lee22. OIB – Ocean-island basalt; E- and N-MORB – enriched and normal mid-ocean-ridge basalt. Data sources are provided in Table S1.

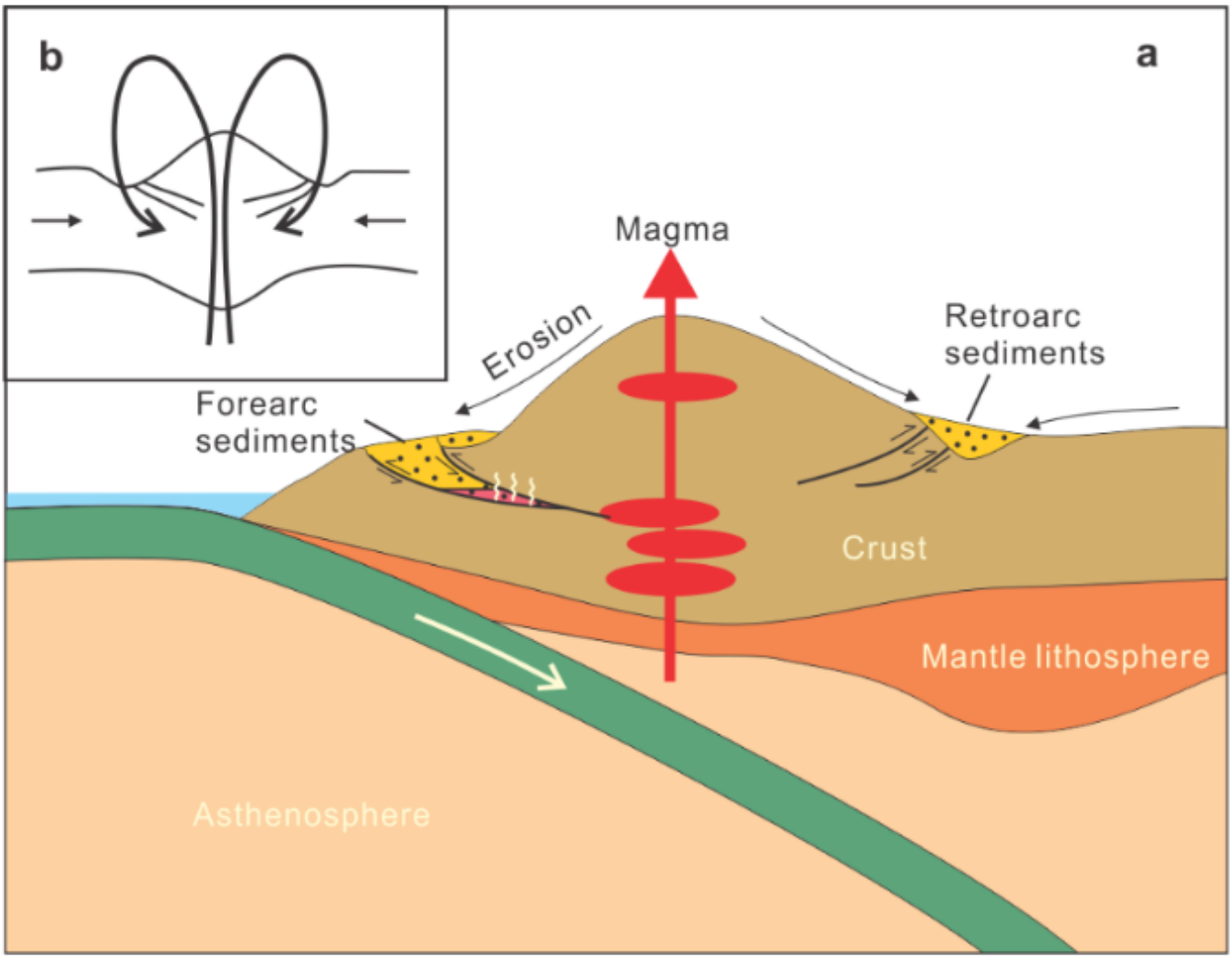

Figure 4

Cartoon showing rapid endogenic recycling of arc magmatic rocks through thrust channels in continental arcs (not to scale).

Supplementary Files

This is a list of supplementary files associated with this preprint. Click to download.

- SupplementaryFigures.pdf
- SupplementaryTableS1.xlsx
- SupplementaryTableS2.xlsx
- SupplementaryTableS3.xlsx
- SupplementaryTableS4.xlsx